TRENDS IN SCIENCES 2026; 23(1): 11009
https://doi.org/10.48048/tis.2026.11009 RESEARCH ARTICLE

Nucleon Charge and Magnetization Densities in the Perturbative Chiral Quark Model

Thitiwat Pasukmuang, Kem Pumsa-Ard, Nopmanee Supanam and Patipan Uttayarat*

Theoretical High-Energy Physics and Astrophysics (THEPA) Research Unit, Department of Physics, Srinakharinwirot University, Bangkok 10110, Thailand

(*Corresponding author's email: patipan@g.swu.ac.th)

Received: 20 June 2025, Revised: 12 August 2025, Accepted: 19 August 2025, Published: 15 October 2025

Abstract

This study investigates the distributions of charge and magnetization within the nucleon using the Perturbative Chiral Quark Model (PCQM). Nucleon charge and magnetization densities are intrinsically linked to the Sachs electromagnetic form factors. We calculated these Sachs form factors within the PCQM framework, incorporating excited-state quark propagators up to the 2nd excited state. Our findings reveal that both the influence of the meson cloud surrounding the quarks within the nucleon and the inclusion of excited-state quark propagators contribute significantly to the Sachs form factors. The definitions of the nucleon charge and magnetization densities are dependent on the chosen frame of reference. Accordingly, we calculated these densities in both the rest frame and the infinite momentum frame of the nucleon. Our results demonstrate distribution patterns consistent with those reported in previous studies. Specifically, the neutron spherical charge density in the rest frame is observed to be positive near the center and at large distances, with a negative distribution in the intermediate region. Conversely, in the infinite momentum frame, the neutron charge distribution exhibits a negative core surrounded by a positive region extending away from the center.

Keywords: Nucleon, Nucleon electromagnetic form factors, Sachs form factors, Charge and magnetization densities

Introduction

Nucleon electromagnetic form factors are crucial quantities that encapsulate the fundamental properties of the nucleon, including its magnetic moments, charge, and magnetic radii. The dependence of these form factors on the 4-momentum transfer squared, Q^2, provides insights into the nucleon's electromagnetic structure. Furthermore, the detailed distribution of charge and magnetic moment within the nucleon, encoded in its charge and magnetization densities, can be elucidated through a comprehensive study of the nucleon electromagnetic form factors.

The Sachs form factors, $G_E(Q^2)$ and $G_M(Q^2)$, are commonly employed to represent the electromagnetic form factors of the nucleon, facilitating direct comparison between theoretical predictions and experimental measurements. Experimentally, information on the Sachs form factors can be extracted from the elastic scattering of electrons off nucleons. The improved technique of recoil-polarization data measurement has significantly extended the range of momentum transfer, Q^2. For experimental progress and status, see [1,2]. From a theoretical perspective, various approaches and models can be utilized to calculate the Sachs form factors. At low Q^2, these form factors are directly related to the Fourier transform of the charge and magnetization densities. However, at higher Q^2, these simple relationships are invalid because the effect of nucleon recoil becomes increasingly significant. Furthermore, Lorentz contraction must also be considered at high Q^2. Consequently, the straightforward relationships between the form factors and the charge and magnetization densities via Fourier transformation require modification to incorporate the effects of nucleon recoil and Lorentz contraction.

The static charge and magnetization densities, which characterize the distributions of charge and magnetic moments within the nucleon, are defined in the rest frame of the nucleon [3]. However, the Sachs form factors are defined in the Breit frame, and each value of Q^2 corresponds to a distinct Breit frame for the nucleon. In the Breit frame (or "brick-wall frame"), an incident particle experiences a scattering event such that its final momentum vector is equal in magnitude but opposite in direction to its initial momentum vector. Consequently, for each Q^2, a boost from the corresponding Breit frame to the rest frame is required. As a result, there is no unique relationship between the Sachs form factors and the static charge and magnetization densities. Indeed, when relativistic effects are considered, the static charge and magnetization densities become model-dependent quantities. Alternatively, one may also consider the charge and magnetization densities of the nucleon in the infinite momentum frame [4-6].

In this work, we calculate the static charge and magnetization densities of the nucleon using the Sachs form factors derived from the PCQM. The PCQM has been successfully applied to numerous physical quantities, including the pion-nucleon sigma term [7,8], electromagnetic form factors of the nucleon and octet baryons [9-11], helicity amplitudes of the nucleon-delta electromagnetic transition [12], axial form factor of the nucleon [13], and strangeness form factor of the nucleon [14]. We will investigate the charge and magnetization densities in the rest frame of the nucleon. Furthermore, we will specifically focus on the charge densities in the nucleon's infinite momentum frame.

Materials and methods

The PCQM

The baryon in the PCQM is considered the bound state of 3 valence quarks that form the quark core. Due to spontaneous chiral symmetry breaking, a cloud of pseudoscalar mesons (π, K, η) surrounds the quark core. The model Lagrangian of the PCQM can be written as an effective chiral Lagrangian [7].

$$\mathcal{L}_{eff} = \mathcal{L}_0 + \mathcal{L}_{int}^{str} + \mathcal{L}_{\chi SB} \quad (1)$$

where $\mathcal{L}_0$ comprises the Lagrangian of the massless quark field $\psi(x)$, which is confined by the static effective potential $V_{eff} = S(r) + \gamma^0 V(r)$, and the massless pseudoscalar meson field $\phi_i(x)$. Specifically, $\mathcal{L}_0$ is given by:

$$\mathcal{L}_0 = \bar{\psi}(x)\left[i\gamma^\mu \partial_\mu - \gamma^0 V(r) - S(r)\right]\psi(x) + \frac{1}{2}\sum_{i=1}^{8}\left[\partial_\mu \phi_i(x)\right]^2. \quad (2)$$

$\mathcal{L}_{int}^{str}$ describes the interaction between quarks and pseudoscalar mesons. To the lowest order, it is given by:

$$\mathcal{L}_{int}^{str} = -\bar{\psi}(x)S(r)i\gamma^5 \frac{\hat{\phi}(x)}{F}\psi(x), \quad (3)$$

where the pseudoscalar meson matrix $\hat{\phi}$ is given by:

$$\frac{\hat{\phi}}{\sqrt{2}} = \sum_{i=1}^{8}\frac{\phi_i \lambda_i}{2} = \begin{pmatrix} \frac{\pi^0}{\sqrt{2}} + \frac{\eta}{\sqrt{6}} & \pi^+ & K^+ \\ \pi^- & -\frac{\pi^0}{\sqrt{2}} + \frac{\eta}{\sqrt{6}} & K^0 \\ K^- & \bar{K}^0 & -\frac{2\eta}{\sqrt{6}} \end{pmatrix}, \quad (4)$$

with $F = 88$ MeV being the pion decay constant in the chiral limit [15]. The Lagrangian $\mathcal{L}_{\chi SB}$ contains the explicit chiral symmetry breaking terms, resulting from the mass of the quark and the pseudoscalar meson fields. Specifically,

$$\mathcal{L}_{\chi SB} = -\bar{\psi}(x)\mathcal{M}\psi(x) - \frac{B}{2}Tr\left[\hat{\phi}^2(x)\mathcal{M}\right], \quad (5)$$

where $\mathcal{M} = diag\{\hat{m}, \hat{m}, m_s\}$ represents the diagonal light current quark mass matrix. Here, we restrict to the isospin-symmetric case where $\hat{m} = (m_u + m_d)/2$. In the PCQM, the quark masses are chosen to be $\hat{m} = 7$ MeV and $m_s = 25\hat{m}$ [7]. In terms of the quark masses $\hat{m}$ and m_s, the pseudoscalar meson masses can be represented by the relations:

$$M_\pi^2 = 2\hat{m}B, \quad M_K^2 = (\hat{m} + m_s)B, \quad M_\eta^2 = \frac{2}{3}(\hat{m} + 2m_s)B, \quad (6)$$

where B is the quark condensate parameter and the value of B is chosen to be 1.4 GeV [7]. It should be noted that these relations for the pseudoscalar meson masses satisfy the Gell-Mann-Oakes-Renner and the Gell-Mann-Okubo relations.

The interaction between the quark and the pseudoscalar meson modifies the mass and charge of the nucleon. To restore the physical charges of both the proton and neutron, renormalization of the PCQM is required. The counterterm technique is employed within the PCQM to ensure the correct charge of the nucleon. Consequently, at the 1-loop level of the quark-pseudoscalar meson interaction, the quark field $\psi(x)$ is also renormalized to yield the renormalized quark field $\psi^r(x)$. In addition, the quark masses $\hat{m}$ and m_s are likewise renormalized, becoming the renormalized quark masses $\hat{m}^r$ and m_s^r, respectively. As a result, the Lagrangian of the model is also renormalized. A comprehensive account of the PCQM renormalization process can be found in [9].

Instead of explicitly introducing the confined effective potential V_{eff}, the PCQM posits that the ground state of the quark wave function, $u_0(\vec{x})$, can be described by the Gaussian ansatz of the form:

$$u_0(\vec{x}) = N_0 \exp\left(-\frac{\vec{x}^2}{2R^2}\right)\begin{pmatrix}1\\ i\rho\frac{\vec{\sigma}\cdot\vec{x}}{R}\end{pmatrix}\chi_s\chi_f\chi_c, \quad (7)$$

where N_0 is the normalization factor, χ_s, χ_f, and χ_c are the quark spin, flavor, and color wavefunctions respectively. The utilization of the Gaussian ansatz allows for analytical calculations within the PCQM. By taking $\int d^3x\, u_0^\dagger(\vec{x})u_0(\vec{x}) \equiv 1$ as the normalization condition, 1 gets:

$$N_0 = \left[\pi^{3/2}R^3\left(1+\frac{3\rho^2}{2}\right)\right]^{-1/2}. \quad (8)$$

Here, R and ρ are the model parameters. The quark wave function $u_0(\vec{x})$ satisfies the Dirac equation:

$$\left[-i\vec{\alpha}\cdot\vec{\nabla} + \beta\, S(r) + V(r) - \mathcal{E}_0\right]u_0(\vec{x}) = 0, \quad (9)$$

where $\mathcal{E}_0$ represents the ground state energy of the quark confined within the baryon. It is noteworthy that the explicit forms of the potentials $S(r)$ and $V(r)$ can be derived by substituting $u_0(\vec{x})$ back into the Dirac equation. Both potentials are found to assume the form of harmonic oscillator potentials [7]:

$$S(r) = M_1 + c_1 r^2, \quad V(r) = M_2 + c_2 r^2, \quad (10)$$

where

$$M_1 = \frac{1-3\rho^2}{2\rho R}, M_2 = \mathcal{E}_0 - \frac{1+3\rho^2}{2\rho R}, c_1 = c_2 = \frac{\rho}{2R^3}. \quad (11)$$

Early work on the PCQM [7,9] simplifies calculations by assuming that the contribution of the quark propagator, $iG_\psi(x,y)$, arises purely from the ground state quark wave function, $u_0(\vec{x})$. This is expressed as:

$$iG_\psi(x,y) = u_0(\vec{x})\bar{u}_0(\vec{y})\exp[-i\mathcal{E}_0(x_0-y_0)]\theta(x_0-y_0). \quad (12)$$

Consequently, all quark wave functions in the excited states are discarded. As a result, R and ρ function as the model parameters. Rather than fixing R and ρ to specific experimental data, their values are deduced from the axial coupling constant g_A of the nucleon calculated in the zero-order (the 3-quark core) approximation and the leading order proton square charge radius $\langle r_E^2\rangle_{LO}$, with the explicit forms:

$$g_A = \frac{5}{3}\left(1 - \frac{2\rho^2}{1+\frac{3}{2}\rho^2}\right), \quad (13)$$

and

$$\langle r_E^2\rangle_{LO} = \frac{3R^2}{2}\left(\frac{1+\frac{5}{2}\rho^2}{1+\frac{3}{2}\rho^2}\right). \quad (14)$$

with $g_A = 1.25$ chosen for the zero-order calculation, the parameter ρ is fixed at $\rho = \sqrt{2/13}$. Given the approximated value of $\langle r_E^2\rangle_{Lo}$ ranges from 0.5 to 0.7 fm^2, the value of parameter R falls between 0.55 and 0.65 fm. Therefore, we take $\rho = \sqrt{2/13}$ and $R =$ 0.60 fm as the central values of the model parameters. The uncertainty in the model predictions can be estimated by allowing R to vary from 0.55 to 0.65 fm. Notably, with this approach, the PCQM is considered a parameter-free model.

The PCQM was later extended to incorporate specific excited quark states into the quark propagator. The inclusion of excited quark states, up to the 2nd level, was initially introduced in the study of the nucleon to delta electromagnetic transition [12]. By utilizing the

explicit forms of the potentials $S(r)$ and $V(r)$ in Eq. (10), the excited-state quark wave functions $u_\alpha(\vec{x})$ can be determined. Here, α denotes the set of quantum numbers specifying the quark state. A quark in the state α with energy $\mathcal{E}_\alpha$ has a wave function of the form:

$$u_\alpha(\vec{x}) = N_\alpha \exp\left(-\frac{\vec{x}^2}{2R_\alpha^2}\right)\begin{pmatrix} g_\alpha(r) \\ i\vec{\sigma}\cdot\hat{x}\, f_\alpha(r)\end{pmatrix}\mathcal{Y}_\alpha(\hat{x})\chi_f\chi_c, \quad (15)$$

where N_α is the normalization constant, and the wave function satisfies $\int d^3x\, u_\alpha^\dagger(\vec{x})u_\alpha(\vec{x}) = 1$. Here, $r \equiv |\vec{x}|$, and $\mathcal{Y}_\alpha(\hat{x})$ represents the angular dependence arising from the coupling between the quark angular momentum and spin in the state α. The upper and lower components of the quark spinor are denoted by $g_\alpha(r)$ and $f_\alpha(r)$, respectively. It is important to note that there are 2 parameters, ρ_α and R_α, for each quark in the state α and both parameters appear within $g_\alpha(r)$ and $f_\alpha(r)$ [10,12]. However, within the PCQM, there exist constraints that relate ρ_α and R_α to the ground-state parameters ρ and R. Consequently, extending the PCQM to include the excited-state quark propagator does not introduce new parameters. The parameters ρ and R remain the fundamental model parameters of the PCQM. The full quark propagator, incorporating excited quark states, is given by:

$$iG_\psi(x,y) = \theta(x_0 - y_0)\sum_\alpha u_\alpha(\vec{x})\bar{u}_\alpha(\vec{y})\exp[-i\mathcal{E}_\alpha(x_0 - y_0)]. \quad (16)$$

In the PCQM, the standard free Feynman propagator is employed as the meson propagator:

$$i\Delta_{ij}(x-y) = \delta_{ij}\int \frac{d^4k}{(2\pi)^4 i}\frac{\exp[-ik(x-y)]}{M_\Phi^2 - k^2 - i\epsilon}, \quad (17)$$

where M_Φ represents the mass of the pseudoscalar mesons (π, K, η).

The Sachs form factors in the PCQM

The Sachs form factors for the nucleon N (where $N = p$ for proton and $N = n$ for neutron) in the PCQM up to 2nd order $(n = 2)$ can be obtained from the following relations:

$$\chi_s^\dagger \chi_s G_E^N(Q^2) = \left\langle \phi_0 \middle| \sum_{n=0}^{2}\frac{i^n}{n!}\int \delta(t)\, d^4x d^4x_1 \dots d^4x_n e^{-iq\cdot x} T[\mathcal{L}_r^{str}(x_1)\dots\mathcal{L}_r^{str}(x_n) j_r^0(x)]\middle|\phi_0\right\rangle, \quad (18)$$

where, $\mathcal{L}_r^{str} = \mathcal{L}_{int}^{str} + \delta\mathcal{L}^{str}$ is the renormalized strong-interaction Lagrangian, which includes the counterterms and

$$\chi_s^\dagger\, i\frac{\vec{\sigma}_N\times\vec{q}}{2m_N}\chi_s G_M^N(Q^2) = \left\langle \phi_0 \middle| \sum_{n=0}^{2}\frac{i^n}{n!}\int \delta(t)\, d^4x d^4x_1 \dots d^4x_n e^{-iq\cdot x} T[\mathcal{L}_r^{str}(x_1)\dots\mathcal{L}_r^{str}(x_n)\vec{j}_r(x)]\middle|\phi_0\right\rangle. \quad (19)$$

The renormalized electromagnetic current operator j_r^μ is obtained through minimal substitution. In the PCQM, j_r^μ can be expressed as:

$$j_r^\mu = j_{\psi^r}^\mu + j_\phi^\mu + \delta j_{\psi^r}^\mu, \quad (20)$$

where

$$j_{\psi^r}^\mu = \bar{\psi}^r\gamma^\mu Q\psi^r, \quad (21)$$

and

$$j_\phi^\mu = \left(f_{3ij} + \frac{f_{8ij}}{\sqrt{3}}\right)\phi_i\partial^\mu\phi_j, \quad (22)$$

with f_{ijk} being the totally antisymmetric structure constants of SU(3). The currents $j_{\psi^r}^\mu$ and j_ϕ^μ represent the interactions of a photon with a quark field and a pseudoscalar meson field, respectively. The renormalized current operator $\delta j_{\psi^r}^\mu$ is given by:

$$\delta j_{\psi^r}^\mu = \bar{\psi}^r(Z-1)\gamma^\mu Q\psi^r, \quad (23)$$

where $Z = diag\{Z_u,\ Z_d,\ Z_s\}$ is the renormalization constant matrix, which ensures the correct physical charges for both proton and neutron. Here, our analysis is restricted to the isospin-symmetric case, i.e., $Z_u = Z_d$.

The relevant diagrams contributing to the Sachs form factors in the PCQM are illustrated in **Figure 1**. The quark propagator is present in 2 diagrams: The meson cloud diagram (c) and the vertex correction diagram (d). In the study of the Sachs form factor within

the PCQM, the inclusion of the excited-state quark propagator was initially explored in the context of the neutron charge form factor, as described in [10]. The aim of this initial investigation was to determine whether the excited-state quark propagator could improve the small values observed for the neutron charge form factor. However, the inclusion of the excited-state quark propagator was not applied to the proton at that time. Subsequently, in [16], both the proton and neutron were treated on an equal footing by incorporating the excited-state quark propagator into the Sachs form factors of the nucleon. Based on these previous studies, it should be emphasized that both the contributions from the pseudoscalar meson cloud and the inclusion of the excited-state quark propagator are crucial for determining physical observables within the PCQM.

In this work, we incorporate excited quark states in the quark propagator up to the 2nd excitation level, consistent with the methodology outlined in [16]. While the inclusion of higher excited states is, in principle, feasible, it would lead to a rapid increase in the number of diagrams. Therefore, as an initial exploration of the charge and magnetization densities of the nucleon within the PCQM framework, we limit our current investigation to quark propagator including up to the 2nd excited states. The spectrum of the quark states is described by the $S(r)$ and $V(r)$ potentials, which are denoted in Eq. (10). Specifically, the quark ground state is the $1s_{1/2}$ state. The 1st excited state comprises the $1p_{1/2}$ and $1p_{3/2}$ states, while the 2nd excited state includes the $1d_{3/2}$, $1d_{5/2}$, and $2s_{1/2}$ states.

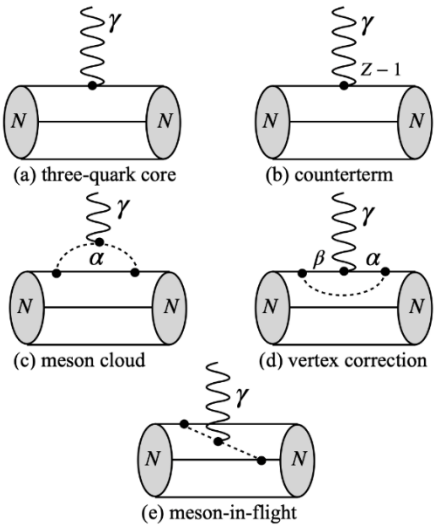

Figure 1 The Feynman diagrams for the Sachs form factors in the PCQM: 3-quark core (a), counterterm (b), meson cloud (c), vertex correction (d), and meson-in-flight (e), where $N = p$ for proton and $N = n$ for neutron.

The nucleon charge and magnetization densities

The spherical charge and magnetization densities, $\rho_E^N(r)$ and $\rho_M^N(r)$ in the rest frame of the nucleon, can be derived from the Sachs form factors, $G_E^N(Q^2)$ and $G_M^N(Q^2)$ [3]. The intrinsic form factors, $\tilde{\rho}_E^N(r)$ and $\tilde{\rho}_M^N(r)$, are related to $G_E^N(Q^2)$ and $G_M^N(Q^2)$ through the following relations

$$\tilde{\rho}_E^N(k) = G_E^N(Q^2)(1+\tau_N)^{\lambda_E}, \quad (24)$$

and

$$\tilde{\rho}_M^N(k) = \frac{G_M^N(Q^2)}{\mu_N}(1+\tau_N)^{\lambda_M}, \quad (25)$$

where μ_N represents the magnetic moment of the nucleon and $\tau_N = Q^2/4m_N$. The reduced spatial frequency, k, is defined as:

$$k^2 = \frac{Q^2}{1+\tau_N}. \quad (26)$$

The λ_E and λ_M are model-dependent parameters. For instance, [17] utilized values of $\lambda_E = 0$ and $\lambda_M = 1$ based on the relativistic soliton model. Conversely, the

cluster model [18] employed $\lambda_E = 1$ and $\lambda_M = 1$. Considering the scaling relations of perturbative QCD at large Q^2, the preferable choices of $\lambda_E = 2$ and $\lambda_M = 2$ were adopted [19].

The spherical charge and magnetization densities, $\rho^N_{E,M}(r)$, in the rest frame of the nucleon can be calculated using the relation:

$$\rho^N_{E,M}(r) = \frac{2}{\pi}\int_0^\infty dk k^2 j_0(kr)\,\tilde{\rho}^N_{E,M}(k), \quad (27)$$

where $j_0(kr)$ denotes the zeroth spherical Bessel function.

Alternatively, as discussed in [4-6], the transverse charge density of protons and neutrons in the infinite momentum frame can be calculated using the following expression:

$$\rho^N_{\perp E}(b) = \frac{1}{2\pi}\int_0^\infty dQQ\; J_0(Qb)\frac{G^N_E(Q^2) + \tau_N G^N_M(Q^2)}{1+\tau_N}, \quad (28)$$

where b represents the transverse distance and J_0 is the zeroth-order cylindrical Bessel function.

Results and discussion

Based on calculations of the Sachs form factors within the PCQM, incorporating the excited-state quark propagator up to the 2nd excited states as detailed in [16], and utilizing parameter values of $\rho = 0.55$ and $R = 0.60$ fm, the proton magnetic moment (μ_p) and neutron magnetic moment (μ_n) were reported as $\mu_p = 2.728$ and $\mu_n = -1.958$ (in the unit of nuclear magneton). Experimental data from the Particle Data Group are $\mu_p = 2.793$ and $\mu_n = -1.913$ [20]. In the present work, we refine these magnitudes, achieving closer agreement with experimental data by employing parameter values of $\rho = 0.65$ and $R = 0.56$ fm, which yield $\mu_p = 2.762$ and $\mu_n = -1.927$. Analytic expressions for all the Sachs form factors are not presented here; interested readers are referred to [16] for details.

The Q^2 dependence of the proton charge form factor $G^p_E(Q^2)$ is presented in **Figure 2**. A comparison of $G^p_E(Q^2)$ with the dipole form factor, $G_D(Q^2) = 1/(1 + Q^2/0.71)^2$, reveals that $G^p_E(Q^2)$ exhibits a more rapid decrease. Within the framework of the PCQM, this observation is attributed to the utilization of a Gaussian ansatz in our calculations. The exponential factor within the Gaussian ansatz results in a more rapid decline of $G^p_E(Q^2)$ as Q^2 increases. Consequently, the Sach form factors exhibit a rapid decrease with increasing Q^2. Furthermore, a decomposition of $G^p_E(Q^2)$ into contributions from the 3-quark core and the surrounding meson cloud is also presented. Consistent with perturbative treatments of the meson cloud in the PCQM, the predominant contribution originates from the 3-quark core.

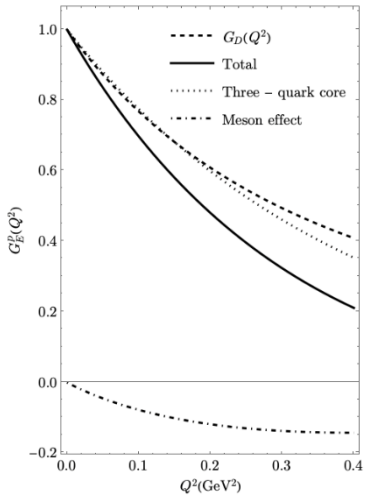

Figure 2 The proton charge form factor $G_E^p(Q^2)$. The solid line represents the total proton charge form factor within the PCQM, incorporating contributions from both the ground state and excited states of the quark propagators. For comparison, the form factor in the dipole approximation $G_D(Q^2)$ is shown by the dashed line. The dotted and the dotted-dashed lines denote the decomposition of $G_E^p(Q^2)$ into contributions from 3-quark core and the meson cloud effect, respectively.

The neutron charge form factor, $G_E^n(Q^2)$ is presented in **Figure 3**. The predicted values of $G_E^n(Q^2)$ within the PCQM are considerably lower than the experimental data. This discrepancy is attributed to the use of a Gaussian ansatz in the calculation, which exhibits a rapid decrease with increasing Q^2. Furthermore, the absence of a 3-quark core contribution to $G_E^n(Q^2)$ means that the entire contribution originates solely from meson effects. Consequently, treating the meson cloud perturbatively results in a small contribution to $G_E^n(Q^2)$.

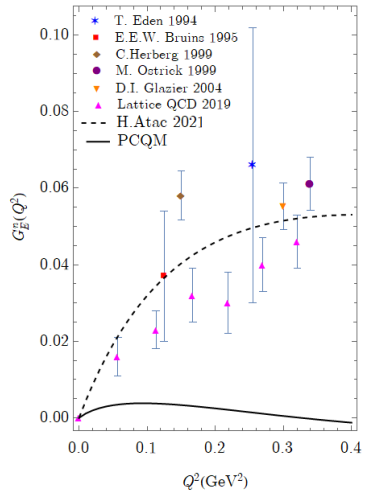

Figure 3 The neutron charge form factor $G_E^n(Q^2)$. The solid line represents the total proton charge form factor within the PCQM, incorporating contributions from both the ground state and excited states of the quark propagators. The dashed line represents the results in [6]. The experimental results and those obtained from lattice QCD are taken from references [21-26].

The proton and neutron magnetic form factors, $G_M^p(Q^2)$ and $G_M^n(Q^2)$, are shown in **Figure 4**. The individual contributions of the 3-quark core and the meson effect to the total magnetic form factors are also presented. For $G_M^p(Q^2)$ within the PCQM, 76.70% of the proton magnetic moment, $\mu_p = G_M^p(0)$, originates from

the 3-quark core, while 23.30% is attributed to the meson effect. This underscores the significance of the meson effect, consistent with findings in previous PCQM studies. Furthermore, the contributions to the neutron magnetic moment, $\mu_n = G_M^n(0)$, from the 3-quark core and the meson effect are 73.28% and 26.72%, respectively.

The significant contribution of excited quark states to the nucleon magnetic moment, as reported in [10,12,16], highlights the necessity of their inclusion in the quark propagator. The incorporation of these excited states contributes approximately 9% to both the proton and neutron magnetic moments, relative to the total contribution. Although the primary contribution to the nucleon magnetic moment originates from the ground state quark propagator, this finding underscores the importance of including excited quark states within the quark propagator in the framework of the PCQM. In the present study, using our selected parameters of $\rho = 0.65$ and $R = 0.56$ fm, which differ slightly from those in [16], the contribution from excited quark states is found to be 11.8% for the proton magnetic moment and 12.2% for the neutron magnetic moment. These contributions are of a similar order of magnitude to those reported in [10,16]. **Table 1** provides a detailed breakdown of the contributions from both the ground-state and excited-state quark propagators to the nucleon magnetic moments. It should be noted that our calculated proton and neutron magnetic moments exhibited relative errors of 1.11% and 0.73%, respectively, when compared to the experimental data [20].

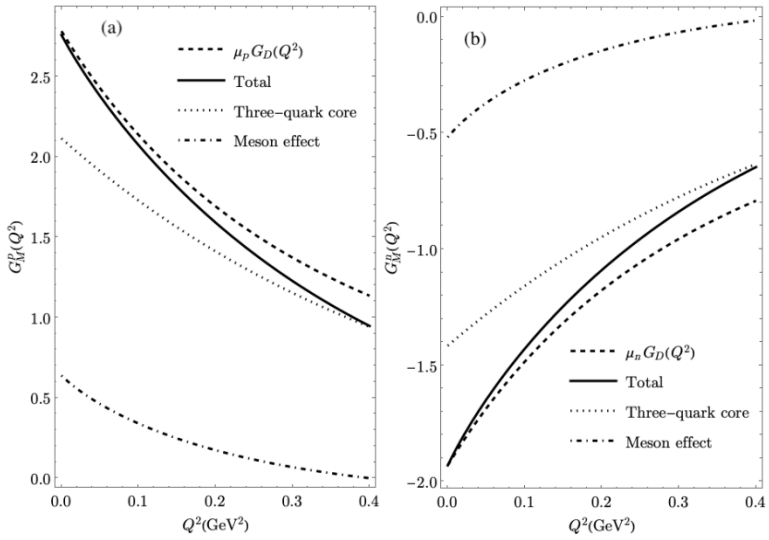

Figure 4 Displays of the proton magnetic form factor $G_M^p(Q^2)$ (a) and the neutron magnetic form factor $G_M^n(Q^2)$ (b). The solid lines represent the total proton and neutron magnetic form factors within the PCQM, incorporating contributions from both the ground state and excited states of the quark propagators. For comparison, the form factors in the dipole approximation are shown by the dashed lines. The dotted and the dotted-dashed lines denote the decomposition of $G_M^{p,n}(Q^2)$ into contributions from 3-quark core and the meson cloud effect, respectively.

Table 1 Decomposition of the total contribution of the nucleon magnetic moment into components arising from the ground-state and excited-states quark propagators.

	Ground state contribution	**Excited states contribution**	**Total contribution**	**Percentage contribution of excited states**	**Exp. [20]**
μ_p	2.4354	0.3264	2.762	11.8%	2.793
μ_n	–1.6921	–0.2351	–1.927	12.2%	–1.913

The Sachs form factors derived from the aforementioned calculations will be employed to determine the spherical charge density, $\rho_E^N(r)$, and the magnetization density, $\rho_M^N(r)$, of the nucleon. It is important to note that these densities are defined in the rest frame of the nucleon. Utilizing the definition provided in Eq. (27), the resulting spherical charge densities for proton and neutron, respectively, are presented in **Figure 5** for the case $\lambda_E = 0, 1, 2$.

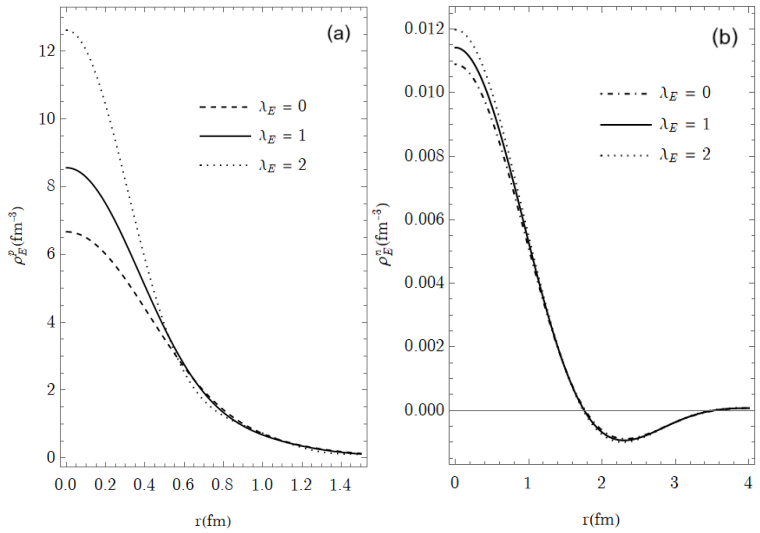

Figure 5 The spherical charge densities of proton **(**a) and neutron (b). The dashed lines represent the results for $\lambda_E = 0$, while the solid and dotted lines correspond to $\lambda_E = 1$ and $\lambda_E = 2$, respectively.

The small r region, measured from the center of the nucleon, is where relativistic corrections become significant. Variations in the model-dependent parameter λ_E lead to different values for the spherical charge distributions $\rho_E^p(r)$ and $\rho_E^n(r)$. This effect is particularly evident in the case of $\rho_E^p(r)$. The proton charge distribution is exclusively positive. In contrast, since the neutron has 0 net charge, its charge distribution comprises positive regions at small and large r and a negative region at intermediate r. Our findings exhibit similar distribution patterns to those presented in [3]. However, discrepancies exist in the amplitude of both $\rho_E^p(r)$ and $\rho_E^n(r)$. This is attributable to the sensitivity of the spherical charge densities to the specific Sachs form factors employed in the calculations.

Alternatively, the radial charge densities can be defined as $r^2\rho_E^p(r)$ and $r^2\rho_E^n(r)$ for proton and neutron respectively. However, in the context of radial charge densities, relativistic corrections are not readily apparent. This is because the r^2 factor tends to diminish the radial charge densities in the small r region. For the proton radial charge density, varying values of λ_E induce oscillatory behavior in the large r region, as illustrated in **Figure 6**. Conversely, for the neutron radial charge density, this oscillatory behavior is less prominent.

The proton and neutron magnetization densities, $\rho_M^p(r)$ and $\rho_M^n(r)$, which represent the magnetic moment distributions within the nucleon, are presented in **Figure 7**. Both densities exhibit similar trends, with relativistic effects observable in the small r region. The corresponding radial magnetization densities, $r^2\rho_M^p(r)$ and $r^2\rho_M^p(r)$, are depicted in **Figure 8**. Oscillatory behavior is evident in the large r region, consistent with the observations in [3].

It is noteworthy that despite the use of different Sachs form factors in this work compared to [3], the general shapes of our charge and magnetization densities are in agreement with the results reported in [3]. Furthermore, our findings also align with those presented in [27], which describes a modification of the PCQM to incorporate higher order interactions between quarks and mesons derived from Chiral Perturbation Theory.

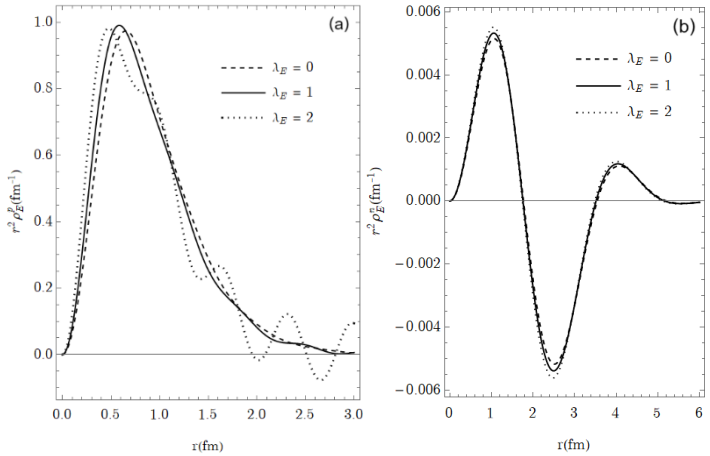

Figure 6 The radial charge densities of proton (a) and neutron (b). The dashed lines represent the results for $\lambda_E = 0$, while the solid and dotted lines correspond to $\lambda_E = 1$ and $\lambda_E = 2$, respectively.

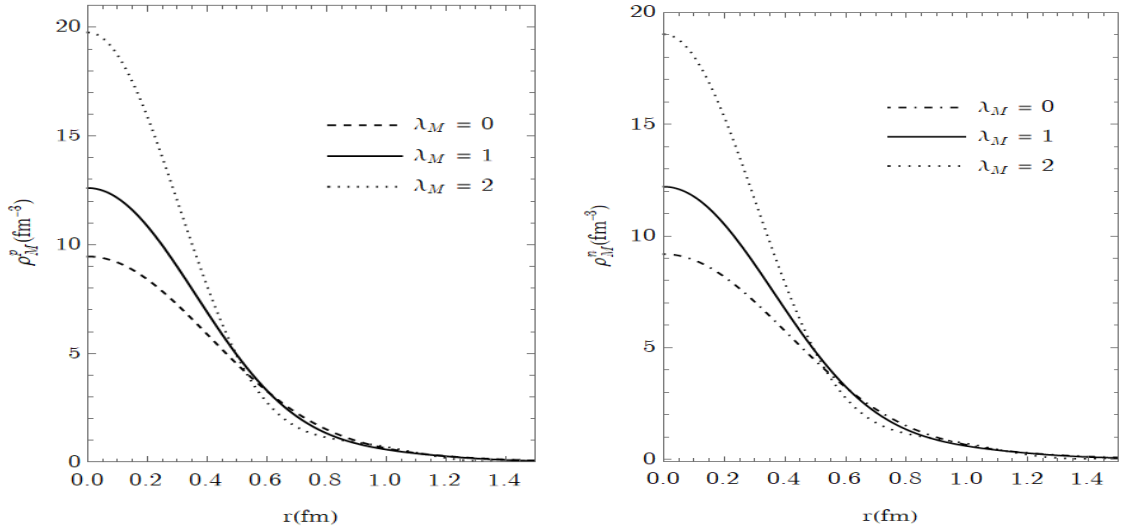

Figure 7 The spherical magnetization densities of proton (a) and neutron (b). The dashed lines represent the results for $\lambda_M = 0$, while the solid and dotted lines correspond to $\lambda_M = 1$ and $\lambda_M = 2$, respectively.

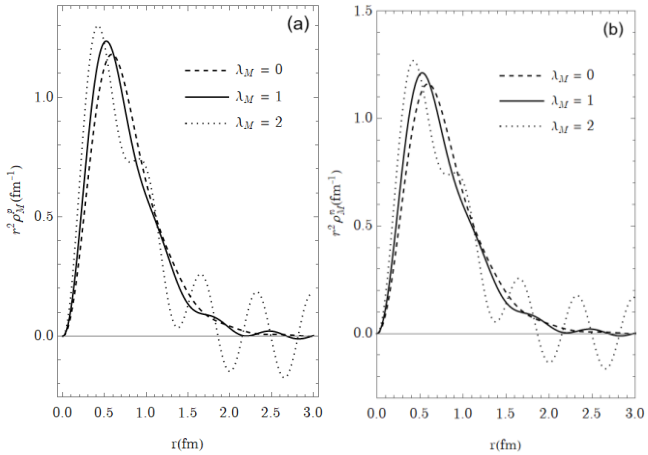

Figure 8 The radial magnetization densities of proton (a) and neutron (b). The dashed lines represent the results for $\lambda_M = 0$, while the solid and dotted lines correspond to $\lambda_M = 1$ and $\lambda_M = 2$, respectively.

Our results for the transverse charge densities of the proton and neutron, $\rho^{p}_{\perp E}(b)$ and $\rho^{n}_{\perp E}(b)$, respectively, within the infinite momentum frame as defined in Eq. (28) are shown in **Figure 9**. Here, b represents the transverse distance. Our findings regarding the transverse charge density patterns align with the analysis conducted by [6], which utilized nucleon form factors under the SU(6) group combined with large- N_c calculation. However, the maximum magnitude of $\rho^{p}_{\perp E}(b)$ at $b = 0$ obtained in this study is approximately 7 times smaller than that reported in [6]. For the neutron, we observe negative values for $\rho^{n}_{\perp E}(b)$ in the small- b region and positive values when $b >$ 0.4 fm, consistent with the observations in [6]. The maximum magnitude of $\rho^{n}_{\perp E}(b)$ at $b = 0$ is approximately 4 times smaller than the central value reported in [6] as shown in **Figure 10**. The transverse charge densities exhibit a strong dependence on the Sachs form factors employed in the calculation.

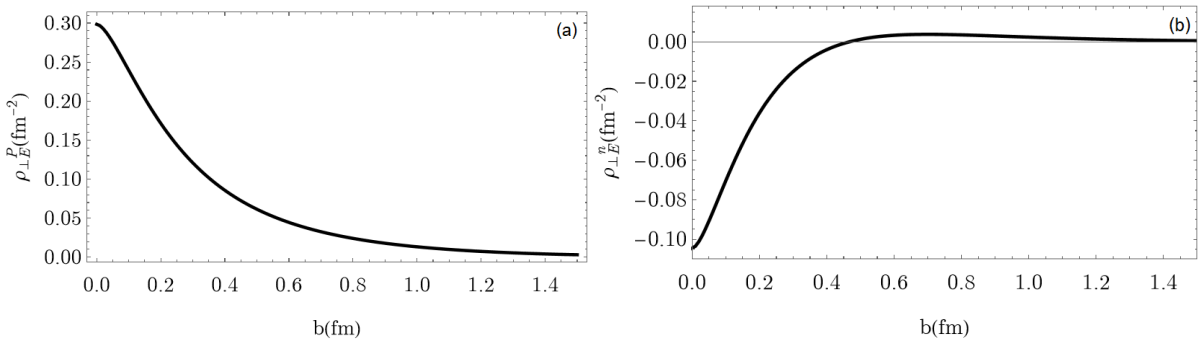

Figure 9 The proton (a) and neutron (b) transverse charge densities.

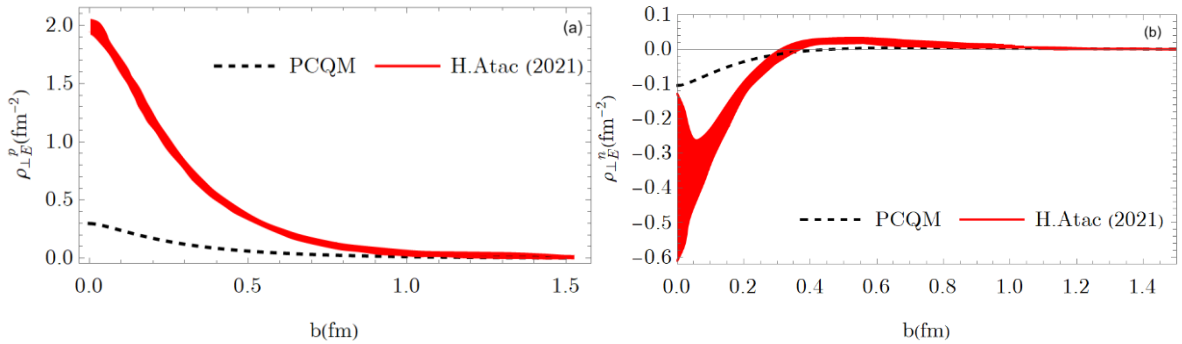

Figure 10 Comparison of our results for the proton (a) and the neutron (b) transverse charge densities with the results in [6].

Figure 11 presents our results for the nucleon transverse charge densities, which are compared to those obtained from the analysis based on the Dispersively Improved Chiral Effective Field Theory (DIχEFT) [28]. Our transverse charge density patterns align with the results reported in [28]; however, we observe smaller amplitudes for both the proton and neutron cases. However, our distribution density $\rho^{n}_{\perp E}(b)$ differs from that presented in [29], which is based on a bound system within a 3 + 1 dimensional Quantum Chromodynamics (QCD) approach. Furthermore, our observed distribution pattern for the density $\rho^{p}_{\perp E}(b)$ deviates slightly from that reported in [30].

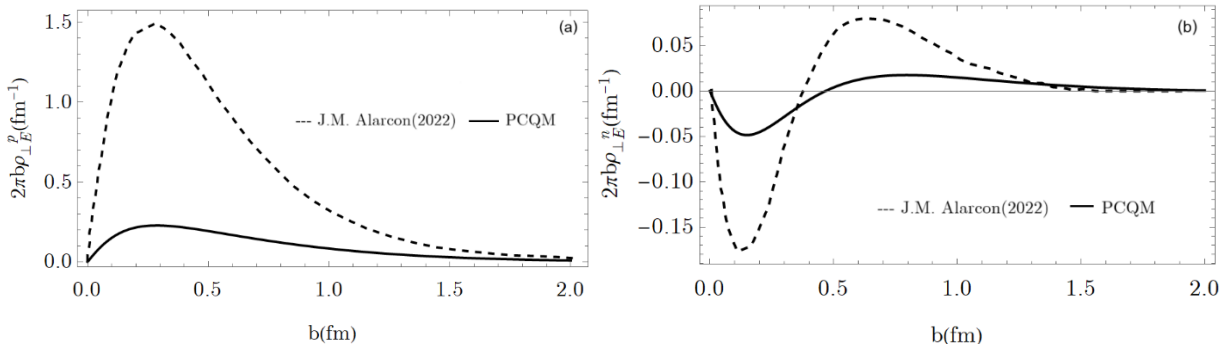

Figure 11 Comparison of our results for the proton (a) and the neutron (b) transverse charge densities with the results in [28].

Finally, it should be noted that attempt has been made to improve the neutron charge form factor within the PCQM by incorporating excited quark states beyond the 2nd level in [31]. However, Liu *et al.* [31] employs a different type of interaction between quarks and pseudoscalar mesons, and different potentials compared to our analysis. It would be insightful to further investigate whether the inclusion of higher excited quark states in the quark propagator can significantly improve the Sachs form factors in our approach.

Conclusions

This study investigates the charge and magnetization densities of the nucleon within the framework of the PCQM. The PCQM allows for the calculation of the nucleon Sachs form factors, which are crucial for determining these densities. Previous PCQM studies often simplified calculations by truncating the quark propagator to its ground state. In this work, we include in the quark propagator up to the 2nd excited quark states. Building upon this, we have refined the Sachs form factor to improve the calculated nucleon magnetic moments. This refinement leads to a new set of optimized parameters $\rho = 0.65$ and $R = 0.56$ fm.

In the PCQM, while the 3-quark core provides the primary contribution to the Sachs form factors and nucleon magnetic moments, the surrounding meson cloud also contributes significantly. In this work, the meson cloud accounts for approximately 23.30% of the proton magnetic moment, and 26.72% of the neutron magnetic moment.

Furthermore, the inclusion of excited quark states in the quark propagator significantly impacts both the Sachs form factors and nucleon magnetic moments. These excited states contribute substantially, accounting for up to 11.8 and 12.2% of the proton and neutron magnetic moments, respectively.

The calculated Sachs form factors are utilized as input for determining the nucleon charge and magnetization densities. For the proton, our calculations demonstrate positive values for both charge and magnetization densities across the entire radial range measured from the center of the proton. Conversely, for the neutron, the magnetization density consistently remains positive. However, the charge density exhibits negative values in the intermediate radial region, becoming positive in both the small and large radial regions. Furthermore, our results indicate that the proton transverse charge density maintains positive values across the entire range of the transverse distance (b), whereas the neutron transverse charge density displays negative values for small b and transitions to positive values with increasing b.

The PCQM highlights the importance of both the meson cloud effect and the inclusion of excited quark states, each providing significant contributions (on the order of 10% for the latter) to various physical observables, including the Sachs form factors and nucleon magnetic moments. Determining the optimal number of excited quark states to include in the PCQM calculations remains an open question. Further research is necessary to refine the PCQM, and we intend to explore this in future investigations.

Acknowledgements

This work was supported by Srinakrarinwirot University (SWU), Thailand and the National Science, Research, and Innovation Fund (NSRF), grant number 046/2568.

Declaration of Generative AI in Scientific Writing

The authors acknowledge the use of generative AI tool Gemini by Google in the preparation of this manuscript, specifically for language editing and grammar correction. No content generation or data interpretation was performed by AI. The authors take full responsibility for the content and conclusions of this work.

CRediT Author Statement

T Pasukmuang: Writing - Original draft; Methodology; Formal analysis. **K Pumsa-ard:** Writing - Original draft; Conceptualization; Validation. **N Supanam:** Writing - Reviewing and Editing. **P Uttayarat:** Writing - Reviewing and Editing; Validation; Supervision.

References

[1] H Gao, C Peng and ZW Zhao. Experimental progress and status on nucleon electromagnetic form factors. *EPJ Web of Conferences* 2016; **113**, 1012.

[2] G Gilfoyle. Future measurements of the nucleon elastic electromagnetic form factors at Jefferson Lab. *EPJ Web of Conferences* 2018; **172**, 2004.

[3] JJ Kelly. Nucleon charge and magnetization densities from Sachs form factors. *Physical Review C* 2002; **66**, 65203.

[4] GA Miller. Charge densities of the neutron and proton. *Physical Review Letters* 2007; **99**, 112001.

[5] CE Carlson and M Vanderhaeghen. Empirical transverse charge densities in the nucleon and the nucleon-to-Δ transition. *Physical Review Letters* 2008; **100**, 32004.

[6] H Atac, M Constantinou, ZE Meziani, M Paolone and N Sparveris. Measurement of the neutron charge radius and the role of its constituents. *Nature Communications* 2021; **12**, 1759.

[7] VE Lyubovitskij, T Gutsche, A Faessler and EG Drukarev. Sigma-term physics in the perturbative chiral quark model. *Physical Review D* 2001; **63**, 54026.

[8] T Inoue, VE Lyubovitskij, T Gutsche and A Faessler. Updated analysis of meson-nucleon σ terms in the perturbative chiral quark model. *Physical Review C* 2004; **69**, 35207.

[9] VE Lyubovitskij, T Gutsche and A Faessler. Electromagnetic structure of the nucleon in the perturbative chiral quark model. *Physical Review C* 2001; **64**, 65203.

[10] S Cheedket, VE Lyubovitskij, T Gutsche, A Faessler, K Pumsa-ard and Y Yan. Electromagnetic form factors of the baryon octet in the perturbative chiral quark model. *The European Physical Journal A: Hadrons and Nuclei* 2004; **20**, 317-327.

[11] XY Liu, K Khosonthongkee, A Limphirat and Y Yan. Study of baryon octet electromagnetic form factors in perturbative chiral quark model. *Journal of Physics G: Nuclear and Particle Physics* 2014; **41**, 55008.

[12] K Pumsa-ard, VE Lyubovitskij, T Gutsche, A Faessler and S Cheedket. Electromagnetic nucleon-delta transition in the perturbative chiral quark model. *Physical Review C* 2003; **68**, 15205.

[13] K Khosonthongkee, VE Lyubovitskij, T Gutsche, A Faessler, K Pumsa-ard and S Cheedket and Y Yan. Axial form factor of the nucleon in the perturbative chiral quark model. *Journal of Physics G: Nuclear and Particle Physics* 2004; **30**, 793-810.

[14] VE Lyubovitskij, P Wang, T Gutsche and A Faessler. Strange nucleon form factors in the perturbative chiral quark model. *Physical Review C* 2002; **66**, 55204.

[15] J Gasser, ME Sainio and A Švarc. Nucleons with chiral loops. *Nuclear Physics B* 1988; **307(4)**, 779-853.

[16] J Jarassriwilai, K Pumsa-ard and P Uttayarat. Inclusion of the excited states quark propagator to the nucleon electromagnetic form factors in the perturbative chiral quark model. *Results in Physics* 2020; **16**, 103125.

[17] X Ji. A relativistic skyrmion and its form factors. *Physics Letters B* 1991; **254(3-4)**, 456-461.

[18] AL Licht and A Pagnamenta. Wave functions and form factors for relativistic composite particles. II. *Physical Review D* 1970; **2**, 1156.

[19] AN Mitra and I Kumari. Relativistic form factors for clusters with nonrelativistic wave functions. *Physical Review D* 1977; **15**, 261.

[20] C Patrignani, C Schwanda, S Spanier, G Venanzoni, CZ Yuan, K Agashe, G Aielli, BC

Allanach, J Alvarez-Muñiz, M Antonelli, EC Aschenauer, DM Asner, K Assamagan, H Baer, S Banerjee, RM Barnett, L Baudis, CW Bauer, JJ Beatty, J Beringer, ..., PA Zyla. Reviews of particle physics. *Physical Review D* 2024; **110**, 30001.

[21] T Eden, R Madey, WM Zhang, BD Anderson, AR Baldwin, JM Cameron, JM Finn, CC Foster, JJ Kelly, S Kowalski, R Lourie, P Markowitz, B Ni, PJ Pella, J Schambach, M Spraker, E Steinfelds, EJ Stephenson and JW Watson. Performance of a neutron polarimeter to measure the electric form factor of the neutron. *Nuclear Instruments and Methods in Physics Research Section A* 1994; **338(2-3)**, 432-441.

[22] EEW Bruins, TS Bauer, HWD Bok, CP Duif, WCV Hoek, DJJD Lange, A Misiejuk, Z Papandreou, EP Sichtermann, H Reike, D Durek, F Frommberger, R Gothe, D Jakob, G Kranefeld, C Kunz, N Leiendecker, G Pfeiffer, E Jans and J Konijn, ..., H Arenhövel. Measurement of the neutron magnetic form factor. *Physical Review Letters* 1995; **75**, 21-24.

[23] C Herberg, M Ostrick, HG Andresen, JRM Annand, K Aulenbacher, J Becker, P Drescher, D Eyl, A Frey, P Grabmayr, SJ Hall, P Hartmann, T Hehl, W Heil, J Hoffmann, D Ireland, JD Kellie, F Klein, K Livingston, …, R Watson. Determination of the neutron electric form factor in the D$(e, \mathrm{e}'n)$p reaction and the influence of nuclear binding. *The European Physical Journal A* 1999; **5**, 131-135.

[24] M Ostrick, C Herberg, HG Andresen, JRM Annand, K Aulenbacher, J Becker, P Drescher, D Eyl, A Frey, P Grabmayr, P Hartmann, T Hehl, W Heil, J Hoffmann, D Ireland, JD Kellie, F Klein, K Livingston, C Nachtigall, …, R Watson. Measurement of the neutron electric form factor $G_{E,n}$ in the quasifree $^2H(\vec{e}, e'\vec{n})p$ reaction. *Physical Review Letters* 1999; **83**, 276-279.

[25] DI Glazier, M Seimetz, JRM Annand, H Arenhövel, MA Antelo, C Ayerbe, P Bartsch, D Baumann, J Bermuth, R Böhm, D Bosnar, M Ding, MO Distler, D Elsner, J Friedrich, S Hedicke, P Jennewein, GJM Nas, FH Klein, …, M Weis. Measurement of the electric form factor of the neutron at $Q^2 = 0.3 - 0.8\ (\mathrm{GeV/c})^2$. *The European Physical Journal A* 2005; **24**, 101-109.

[26] C Alexandrou, S Bacchio, M Constantinou, J Finkenrath, K Hadjiyiannakou, K Jansen, G Koutsou and AV Aviles-Casco. Proton and neutron electromagnetic form factors from lattice QCD. *Physical Review D* 2019; **100**, 14509.

[27] A Faessler, T Gutsche, VE Lyubovitskij and K Pumsa-ard. Chiral dynamics of baryons in a Lorentz covariant quark model. *Physical Review D* 2006; **73**, 114021.

[28] JM Alarcón and C Weiss. Transverse charge and current densities in the nucleon from dispersively improved chiral effective field theory. *Physical Review D* 2022; **106**, 54005.

[29] T Kurai. Proton and neutron electromagnetic form factors based on bound system in 3 + 1 dimensional QCD. *Journal of Modern Physics* 2020; **11**, 741-765.

[30] AV Gramolin and RL Russell. Transverse charge density and the radius of the proton. *Physical Review D* 2020; **105**, 54004.

[31] XY Liu, A Limphirat, K Xu, D Samart, K Khosonthongkee and Y Yan. Analysis of excited quark propagator effects on neutron charge form factor. *The European Physical Journal A* 2019; **55**, 218.